Chemical Engineering Science 65 (2010) 2382–2391

Contents lists available at ScienceDirect

Chemical Engineering Science

journal homepage: www.elsevier.com/locate/ces

Influence of buoyancy-driven convection on the dynamics of A+B→C reaction fronts in horizontal solution layers

L. Rongy, P.M.J. Trevelyan, A. De Wit *

Nonlinear Physical Chemistry Unit, Service de Chimie Physique et Biologie Théorique, Faculté des Sciences CP 231, Université Libre de Bruxelles (ULB), 1050 Brussels, Belgium

ARTICLE INFO

Article history:
Received 20 April 2009
Received in revised form
6 September 2009
Accepted 10 September 2009
Available online 16 September 2009

Keywords:
Reaction–diffusion–convection
Hydrodynamics
Convection
Buoyancy
Diffusion
Kinetics

ABSTRACT

The dynamics of initially vertical A+B→C reaction fronts propagating in covered horizontal solution layers can be influenced by buoyancy-driven convection. Experiments have provided evidence that a much faster propagation of the front occurs in solutions than that predicted by reaction–diffusion (RD) theories, thereby suggesting the influence of convective effects arising if A, B, and C have different densities. Here we analyze numerically and theoretically the dynamics resulting from the coupling of a simple A+B→C chemical reaction with diffusion and convection induced by density differences across the reaction front. The important parameters of the related reaction–diffusion–convection (RDC) model are the three dimensionless Rayleigh numbers, quantifying the contribution of each species concentration to the density of the solution, the layer thickness, and the initial reactant concentration ratio. The presence of buoyancy-driven convection at the front induces a propagation of this front even in the case of equal diffusion coefficients and equal initial reactant concentrations for which RD theories predict a non-moving front. In the case of equal initial concentrations, even in the presence of convection, the classification of the various possible dynamics and the prediction of the direction of front propagation can be obtained from simple criteria on the Rayleigh numbers. In the case of different initial reactant concentrations for which, in the absence of convection, the RD front propagates towards the side of the less concentrated reactant, the introduction of buoyancy convection not only invalidates the long time RD scalings but can lead to a double reversal in the direction of propagation of the reaction front for intermediate times. The influence of the different parameters on the RDC dynamics is presented.

1. Introduction

The rather simple system of two chemical reactants A and B diffusing (with diffusion coefficients D_a and D_b, respectively) and reacting via the second-order scheme

$$A+B\rightarrow C \tag{1}$$

can sustain a reaction front, i.e. a spatially localized region with non-zero production rate, provided that the two reactants are initially separated in space. This reaction–diffusion system has attracted much research interest in the last two decades since the pioneering work of Gálfi and Rácz (1988). Theoretical studies refer typically to an effectively one-dimensional system (along x) considering a translation symmetry of the problem in the two other dimensions. The initial condition is $a=a_0$, $b=0$ for $x<0$ and $a=0$, $b=b_0$ for $x>0$ where a and b are the concentrations of A and B, respectively. The reactants meet at time $t=0$ at $x=0$, forming a reaction front where the reactants A and B are consumed and the product C is generated.

For an infinite domain and in the asymptotic limit of large times, exact scaling laws characterizing the RD dynamics without convection were derived in the work of Gálfi and Rácz (1988) and in subsequent other theoretical studies including Jiang and Ebner (1990), Cornell et al. (1995), Koza (1996) and Sinder and Pelleg (2000). They found that the position x_f and the width w of the reaction front (defined as the position along x where the production rate is maximum and as the square root of the second moment of the production rate distribution, respectively) scale with time as $x_f\sim t^{1/2}$ and $w\sim t^{1/6}$. It can be shown that actually $x_f=C_f\sqrt{t}$ with the constant $C_f=C_f(b_0/a_0,D_a,D_b)$, so that the motion of the reaction front depends only on the diffusion coefficients of the reactants and on the ratio of their initial concentrations, b_0/a_0, but not on the individual magnitudes of a_0 and b_0, (Danckwerts, 1950; Koza, 1996). Further, Koza (1996) showed that the reaction front eventually propagates towards positive x (i.e. to the right here) if and only if $\sqrt{D_a/D_b}>b_0/a_0$. More recently, these large time RD predictions have been extended to the case of reactants initially separated in immiscible solutions by Trevelyan et al. (2008).

* Corresponding author. Tel.: +32 2650 5774.
E-mail addresses: lrongy@ulb.ac.be (L. Rongy), ptrevely@ulb.ac.be (P.M.J. Trevelyan), adewit@ulb.ac.be (A. De Wit).

0009-2509/$ - see front matter © 2009 Elsevier Ltd. All rights reserved.
doi:10.1016/j.ces.2009.09.022

The scalings of this front refer to the diffusion-limited problem when the chemical reaction is limited by the supply of reactants by diffusion. Therefore, they pertain to the large time limit only, or equivalently to the case of instantaneous reactions (the kinetic constant $k \to \infty$). Taitelbaum and coworkers have addressed the behavior of such systems in the non-diffusion limited or 'short time' regime, showing that such 'early time' behaviors can be characterized by completely different properties (see Taitelbaum et al., 1992; Koza and Taitelbaum, 1996). In the small time limit the position of the reaction front is also given by $x_f = C_f\sqrt{t}$, however, Koza (1996) showed that the constant $C_f = C_f(D_a, D_b)$, i.e. C_f is independent of the initial concentrations a_0 and b_0. One finds that the reaction front initially moves to the right, i.e. $x_f > 0$, if and only if $\sqrt{D_a/D_b} > 1$. However, in the case of equal diffusion coefficients Taitelbaum et al. (1991) found that the small time asymptotic position of the reaction front is now given by $x_f = C_f t^{3/2}$ where $C_f = \sqrt{D_a/(4\pi)}(a_0 - b_0)k$, see Trevelyan (2009).

One notes that a sufficient condition for the RD front to exhibit a change in its direction of motion in the course of time is for $\sqrt{D_a/D_b}$ to lie between 1 and b_0/a_0. However, when b_0/a_0 lies between 1 and $\sqrt{D_a/D_b}$, so that the direction of the reaction front in the small and large time asymptotic limits are the same, Taitelbaum and Koza (2000) found that it is also possible for the reaction front to change direction twice in the intermediate time for a range of parameter values. In the case of equal diffusion coefficients of the reactants no such reversal of the RD reaction front is possible as the speed of the front only depends on b_0/a_0 with the more concentrated reactant continuously propagating into the domain of the less concentrated one and further the front is only stationary if the reactants are initially equally concentrated.

The large time analytical scalings characterizing A+B→C fronts, as well as the asymptotic condition for a stationary front have been verified numerically by simulations of microscopic stochastic two-dimensional (2D) models for both equal and unequal diffusion coefficients, see Jiang and Ebner (1990), Larralde et al. (1992) and Cornell (1995). Several experimental works in gels have validated these RD scalings using A+B→C types of reaction, see Koo et al. (1990), Taitelbaum et al. (1992) and Yen et al. (1996), like for instance the complexation reaction of Cu^{2+} with a substrate studied by Koo and Kopelman (1991) in an agarose gel. More recently, a different type of convection-free experiment carried out by Baroud et al. (2003) in a T-shaped microfluidic reactor has further confirmed these RD scalings using the binding reaction of Ca^{2+} with calcium green. All these experiments are not only in excellent agreement with the theoretical scalings, but the actual positions of the reaction front are very close to the predicted theoretical values.

As seen above, the propagation of A+B→C reaction fronts has mostly been studied in gels to avoid any convective motions. However, some experiments in covered horizontal aqueous solutions yield different results to their gel counterparts even for very thin layers. The complexation of copper ions first studied by Koo and Kopelman in gels was next examined by Park et al. (2001) in a thin horizontal solution. Although their results were in reasonable agreement with the front position scaling of $\sqrt{t}$ and front width scaling of $t^{1/6}$, the experimental front was found to travel faster than theoretically predicted. The presence of convection in this system seems likely so that the reaction is no longer diffusion limited. Such deviations from the classical RD theories have further been made evident recently by Shi and Eckert (2006) in their experimental study of a neutralization reaction front in a horizontal Hele–Shaw cell. The position of the front scales like t^m with $m > 0.5$ and m itself dependent on time. Moreover, the front travels faster than the RD front and its position is found to depend on the individual values of the initial concentrations at a fixed ratio b_0/a_0, as well as on the gap width of the cell. This provides evidence that the RD characteristics of A+B→C fronts break down when the reaction is carried out in solution and suggests that the dynamics of these fronts is influenced by chemically-driven buoyancy convection if A, B and C have different densities.

Although the effects of convection on the propagation of autocatalytic fronts have been widely studied theoretically and numerically (see Vasquez et al., 1994; Vladimirova and Rosner, 2003; Rongy et al., 2007 and references therein), the influence of convection on the dynamics of simpler A+B→C reaction fronts has not been addressed in detail yet. In this framework, Rongy et al. (2008) recently studied the influence of convection in the case where the reactants A and B have equal diffusion coefficients and equal initial concentrations for which the RD analysis predicts a non-moving front. The presence of convection cannot only deform the initially vertical planar front but can also lead to its propagation. Fortunately the dynamics in the presence of convection can be fully predicted from the properties of the simple one-dimensional (1D) RD density profile. Those properties are solely functions of the Rayleigh numbers of the problem, quantifying the influence of each chemical species concentration on the solution density. The various possible RDC dynamics have therefore been classified in a parameter space spanned by the Rayleigh numbers.

In this context, it is the objective of this article to extend the study of Rongy et al. (2008) to the case where the reactants have different initial concentrations corresponding to an underlying moving RD front. In that case, the presence of convection also results in a deformation of the front which can furthermore be accelerated with regard to the RD situation. For some values of the Rayleigh numbers we observe a reversal of the front propagation direction in time due to the presence of convection. We conclude that the scalings in time characterizing the propagation of the RD front are drastically affected by the presence of buoyancy-driven flows.

The article is organized as follows. In the next section, we present the two-dimensional RDC model system and the corresponding governing equations. The incompressible Stokes equations for the velocity of the fluid are coupled to RDC equations for the concentrations of the reactants A, B and of the product C through the three Rayleigh numbers $R_{a,b,c}$. Since the system is characterized by many parameters (initial concentrations of the reactants, diffusion coefficients, Rayleigh numbers and the layer thickness), we keep the diffusion coefficients equal throughout this paper in order to highlight the influence of convection. Indeed we show that the RDC system presents rich behaviors even with equal diffusion coefficients. In Section 3, the various possible types of base state density profiles are considered. In Section 4 we analyze the influence of buoyancy-driven convection on the propagation dynamics and scaling properties of A+B→C fronts with initially separated reactants. Finally, conclusions are presented in Section 5.

2. Model system

We consider a two-dimensional (2D) covered solution layer oriented horizontally in the gravity field g, in which the isothermal A+B→C reaction takes place upon contact between two miscible solutions each containing one of the reactants (see Fig. 1). The miscible solutions with initial concentrations a_0 and b_0, respectively, are brought into contact along a planar vertical interface located at $x = 0$. Upon contact, the reactants start to diffuse and react to produce species C. The two reactants and the product affect the density of the solution, which induces convective motion whenever horizontal density gradients are present. The dynamics of the system is described by the RDC

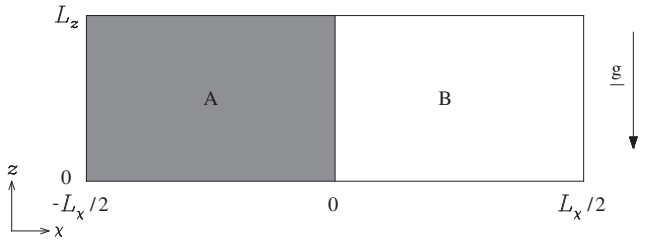

Fig. 1. Sketch of the system.

equations (2)–(4) for the concentrations a, b, c. These are coupled to the 2D incompressible Stokes equation (6) and (7) for the velocity field $\underline{v} = (u, w)$ by a state equation (5) for the diluted solution density ρ assumed to depend linearly on the concentrations. The governing equations thus read

$$\frac{\partial a}{\partial t} + \underline{v}.\underline{\nabla} a = D\nabla^2 a - kab, \tag{2}$$

$$\frac{\partial b}{\partial t} + \underline{v}.\underline{\nabla} b = D\nabla^2 b - kab, \tag{3}$$

$$\frac{\partial c}{\partial t} + \underline{v}.\underline{\nabla} c = D\nabla^2 c + kab, \tag{4}$$

$$\rho(a,b,c) = \rho_0 + \frac{\partial \rho}{\partial a} a + \frac{\partial \rho}{\partial b} b + \frac{\partial \rho}{\partial c} c, \tag{5}$$

$$\underline{\nabla} p = \mu \nabla^2 \underline{v} + \rho(a,b,c)\underline{g}, \tag{6}$$

$$\mathrm{div}\underline{v} = 0, \tag{7}$$

where p denotes the pressure, $\underline{g} = (0, -g)$ is the gravity acceleration acting along z, $\partial\rho/\partial a$, $\partial\rho/\partial b$ and $\partial\rho/\partial c$ are the solutal expansion coefficients assumed constant, and $\rho_0 = \rho(a = 0, b = 0, c = 0)$ is the density of the pure solvent. All chemical species are assumed to have the same constant diffusion coefficient D. The dynamic viscosity μ and the kinetic constant k are assumed constant in space and time. The changes in density are small enough to be neglected except in the buoyancy term $\rho\underline{g}$ of Eq. (5) (Boussinesq approximation).

The evolution equations are made dimensionless by using the characteristic scales of the reaction–diffusion system, i.e. time $\tau_c = 1/ka_0$, length $L_c = \sqrt{D\tau_c}$, velocity $U_c = \sqrt{D/\tau_c}$ and concentration a_0. The pressure is scaled by $p_c = \mu/\tau_c$ and we define a dimensionless pressure gradient including the hydrostatic pressure gradient term as $\underline{\nabla}' p' = \underline{\nabla}' p/p_c - \rho_0 L_c \underline{g}/p_c$ where the primes denote dimensionless variables. The dimensionless density is defined as $\rho' = (\rho - \rho_0)/\rho_c$ where $\rho_c = p_c/L_c g$. Dropping the primes, we obtain the dimensionless governing equations:

$$\frac{\partial a}{\partial t} + \underline{v} \cdot \underline{\nabla} a = \nabla^2 a - ab, \tag{8}$$

$$\frac{\partial b}{\partial t} + \underline{v} \cdot \underline{\nabla} b = \nabla^2 b - ab, \tag{9}$$

$$\frac{\partial c}{\partial t} + \underline{v} \cdot \underline{\nabla} c = \nabla^2 c + ab, \tag{10}$$

$$\underline{\nabla} p = \nabla^2 \underline{v} - (R_a a + R_b b + R_c c)\underline{i}_z, \tag{11}$$

$$\mathrm{div}\underline{v} = 0, \tag{12}$$

where $\underline{i}_z$ is the unit vector along z. The dimensionless Rayleigh numbers $R_{a,b,c}$ are defined as

$$R_i = \frac{\partial \rho}{\partial c_i} \frac{a_0 L_c^3 g}{D\mu}, \tag{13}$$

where c_i is the dimensionless concentration of the corresponding species. The solutal Rayleigh numbers $R_{a,b,c}$ are positive because the corresponding solutes here are all supposed to increase the density of the solvent.

The dimensionless density of the solution is therefore obtained as follows:

$$\rho(x,z,t) = R_a a(x,z,t) + R_b b(x,z,t) + R_c c(x,z,t). \tag{14}$$

We note that the use of Stokes equations is justified by the fact that, in our choice of non-dimensionalization, the inertial terms in the Navier–Stokes equations for the flow field would be divided by a Schmidt number, $S_c = \mu/(\rho_0 D) \approx 10^3$ for small species in water. In a previous study for similar systems Rongy and De Wit (2006) showed that a change in the value of S_c, if taken in this experimental range, does not affect the obtained results, meaning that inertial effects are negligible in these slow flow regimes compared to the viscous effects.

At every boundary of the domain, we require zero-flux boundary conditions for the concentrations. The boundary conditions for the fluid velocity field are rigid walls with no slip on the bottom and top boundaries and slip walls on the left and right ones, i.e.

$$\frac{\partial c_i}{\partial x} = u = \frac{\partial w}{\partial x} = 0 \quad \text{on } x = 0,\ x = L_x, \tag{15}$$

$$\frac{\partial c_i}{\partial z} = u = w = 0 \qquad \text{on } z = 0,\ z = L_z, \tag{16}$$

where L_x and L_z represent, respectively, the dimensionless length and height of the layer. The length of the system and slip walls do not influence the results provided the system is long enough for the reaction front to be unaffected by lateral boundary effects on the time of interest.

The initial conditions are separated reactants such that:

$$a = 1, \quad b = 0, \quad c = 0, \quad \forall\, z, x \le 0,$$
$$a = 0, \quad b = \beta, \quad c = 0, \quad \forall\, z, x > 0,$$

where $\beta = b_0/a_0$. It is therefore sufficient to consider the case $\beta \le 1$ as the case $\beta > 1$ is obtained straightforwardly by symmetry since the transformation $\beta \to 1/\beta$ corresponds to swapping a and b which, along with the transformation $R_a \leftrightarrow R_b$, leaves the system of equations and boundary conditions unchanged. We will therefore only consider the case $\beta < 1$. In the presence of convection the dynamics of the concentration and flow fields are investigated by numerically solving Eqs. (8)–(12) using the numerical procedure described in Rongy et al. (2007). We checked that the results converge while decreasing the time and space step size. The largest domain involved a computational grid of 1024×64 points for $L_x = 1024$ and $L_z = 20$, and a typical time step $dt = 0.1(dz)^2 \sim 9.8 \times 10^{-3}$. For zero Rayleigh numbers, we also recovered the RD results previously obtained (see Gálfi and Rácz, 1988; Jiang and Ebner, 1990; Koza, 1996). We now recall the main characteristics of this RD system in the absence of flow.

When the solution density is unaffected by the chemical reaction (i.e. $R_a = R_b = R_c = 0$), the vertical front propagates in the absence of flow along the x-direction without any deformation and presents thus a translation symmetry along z. Typical concentration profiles are illustrated in Fig. 2 at various times for two values of β obtained by numerical integration of the corresponding RD equations (8)–(10) with $\underline{v} = \underline{0}$. When $\beta = 1$, the reaction front is stationary while when $\beta < 1$, the initial concentration of A is in stoichiometric excess with regard to that of B and hence the front propagates towards the side with the smallest diffusive flux, i.e. the region of the less concentrated reactant B ($x_f > 0$), see Gálfi and Rácz (1988).

As time increases, the concentrations of A and B decrease around the reaction front and the reaction becomes limited by the

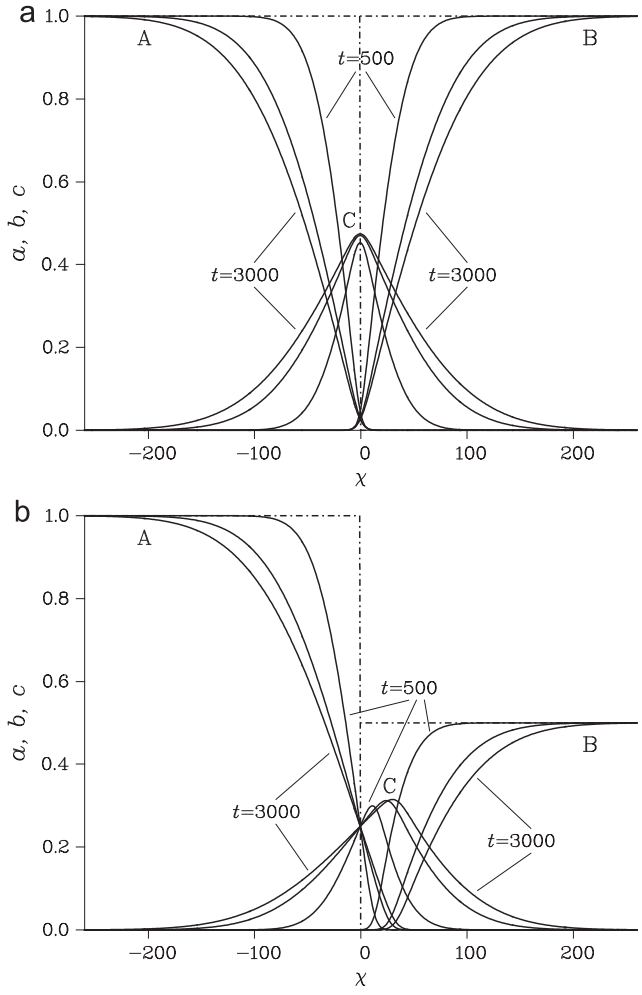

Fig. 2. One-dimensional RD profiles of the concentration of the two reactants, a and b, and of the product, c shown at different times: $t=0$, 500, 2000, and 3000 for (a) $\beta=1$ and (b) $\beta=0.5$. The initial condition is represented by the dot-dashed lines.

supply of reactants by diffusion. Hence, the displacement of the front decreases in time as well as the production rate. The distance between the position of the maximum production rate, x_f, and that of the initial condition, $x=0$, increases as $t^{1/2}$ and the front propagates faster when the difference between the initial concentrations of the reactants increases, i.e. decreasing β.

We note that the dynamics of the reaction front described here is different from that of an autocatalytic front extensively described in the literature and characterized by a permanent shape and a constant propagation speed, see Epstein and Pojman (1998). Such a front results from the interplay between autocatalysis and diffusion while the propagation of a front in A+B→C reaction systems results from the particular choice of the initial condition, i.e. initially segregated reactants.

The goal of the next sections is to analyze the effects of the buoyancy convection induced when A, B and C have different densities on the dynamics and properties of the RD fronts described above. To do so, we first analyze the RD density profiles.

3. Reaction–diffusion density profiles

In the absence of convection, $\underline{v}=\underline{0}$, the RDC system of Eqs. (8)–(10) and the given initial conditions lead to a 1D system of RD equations. The RD density profile is given by $\overline{\rho}(x,t)=R_a\overline{a}(x,t)+R_b\overline{b}(x,t)+R_c\overline{c}(x,t)$ where $\overline{a},\overline{b}$ and $\overline{c}$ are the concentration profiles of the RD system. As it is the horizontal density gradients that initially induce convection one is therefore able to predict the RDC dynamics of the system on the sole basis of the Rayleigh numbers and of the RD concentration profiles. The different behaviors of the RDC system can be analytically classified as functions of $R_{a,b,c}$ without resorting to numerics and further when $\beta=1$ then the direction of front propagation can be found analytically as shown by Rongy et al. (2008). Hence, before examining the RDC system the simple RD system is first analyzed.

Using the same kind of approach as Gálfi and Rácz (1988) the RD system can be simplified. We can write $q(x,t)=\overline{a}+\overline{c}$, with $q_t=q_{xx}$ and $q(-|x|,0)=1$ and $q(|x|,0)=0$. Then using the similarity variable $\eta=x/\sqrt{4t}$ we obtain the solution $q=\frac{1}{2}\mathrm{erfc}(\eta)$. Further, writing $r(x,t)=\overline{b}+\overline{c}$, with $r_t=r_{xx}$ and $r(-|x|,0)=0$ and $r(|x|,0)=\beta$ we can obtain $r=\frac{1}{2}\beta\mathrm{erfc}(-\eta)$. Hence, we have shown that

$$\overline{a}=\frac{1}{2}\mathrm{erfc}(\eta)-\overline{c},\quad \overline{b}=\frac{\beta}{2}\mathrm{erfc}(-\eta)-\overline{c}.$$

One implication of this result is that $\beta\overline{a}+\overline{b}+(\beta+1)\overline{c}=1$. Using Eq. (14) we can then construct the RD density profile

$$\overline{\rho}=\beta R_b+\tfrac{1}{2}(R_a-\beta R_b)\mathrm{erfc}(\eta)+(R_c-R_a-R_b)\overline{c}. \tag{17}$$

One notes that the RD density gradient obtained using the triplet of parameter values (R_a, R_b, R_c) will be identical to the one obtained using the triplet ($R_a+\gamma\beta$, $R_b+\gamma$, $R_c+\gamma(1+\beta)$) for any value of γ with β fixed. Thus, one might anticipate that the flow dynamics for such triplets will be similar as the fluid flow is driven by gradients of the density. Another implication of the RD density profile in Eq. (17) is that the flow pattern obtained using (R_a, R_b, R_c) is identical to the flow pattern obtained using (R_a, R_b, $2R_a+2R_b-R_c$) except that the direction of the fluid flow is now reversed, i.e. the flow field is rotated 180° about the point $x=0$, $z=L_z/2$. These two observations have been checked numerically. Eq. (17) introduces two interesting limiting cases, namely, when $R_c=R_a+R_b$ or when $R_a=\beta R_b$.

The line $R_c=R_a+R_b$ is an interesting case as then C has a density equal to the sum of that of A and B so that the RD density is only a function of η and is antisymmetric about the inflection point at $\eta=0$ even if the reaction front is propagating, see Fig. 3(a). The density profiles vary monotonically between the contribution to density of reactant A, $\rho=R_a$, at $x=-L_x/2$ and the contribution to the density of reactant B, $\rho=\beta R_b$, at $x=L_x/2$. The RD density is a monotonic increasing function of η when $\beta R_b>R_a$ and a monotonic decreasing function of η when $\beta R_b<R_a$. If one introduces the quartet notation (R_a, R_b, R_c, β), then, one notices that the RD density profiles obtained using (R_a, λ/β, $R_a+R\lambda/\beta$, β) are the same for all values of $\beta>0$. with R_a and λ fixed. Further, the RD density gradient obtained using $\lambda+\beta R_b$, R_b, $\lambda+(\beta+1)R_b$, β are the same for all values of β and R_b with λ fixed. These results are an extension of those previously obtained for the case of equal initial reactant concentrations by Rongy et al. (2008).

The line $R_a=\beta R_b$ is another interesting limit as this is the degenerate case when initially the density of the fluid on the left equals that of the fluid on the right, see Fig. 3(b). In this case the density is a linear function of the product concentration. The density profile has a local maximum when $R_c>(1+\beta)R_b$ or a local minimum when $R_c<(1+\beta)R_b$. When $\beta=1$, the reaction front is stationary so that the product distribution is symmetric with regard to $x=0$ and hence so is the density distribution, as stated in Rongy et al. (2008). However, when $\beta\neq1$, the reaction front moves and hence, the local maximum or minimum in the concentration and density both move too, breaking the symmetry of the profile, unlike the case of $\beta=1$. As the reaction front moves

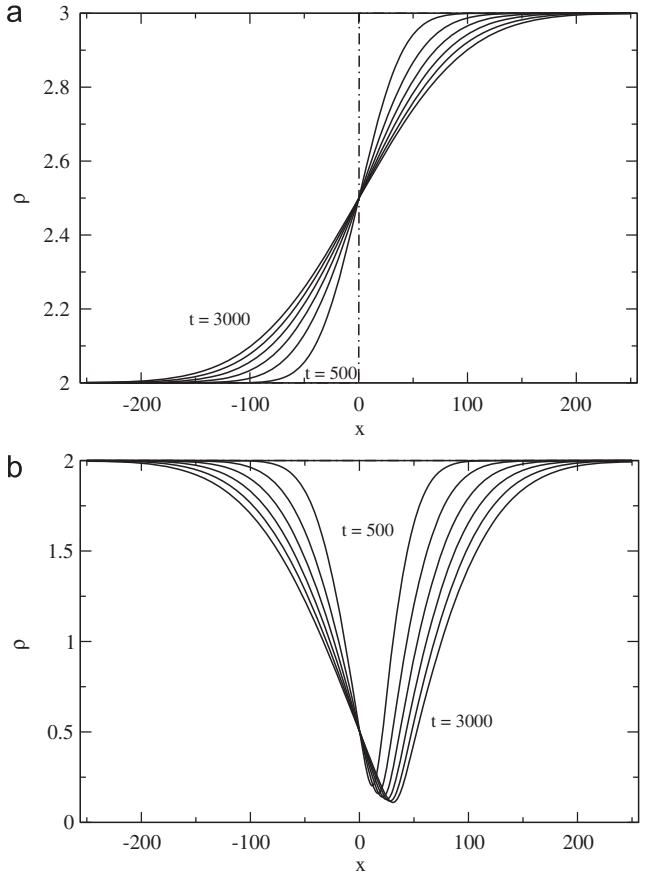

Fig. 3. Reaction–diffusion density profiles along x for $\beta=0.5$ reconstructed following Eq. (14) for (a) $R_c=R_a+R_b$ using $R_a=2$, $R_b=6$, and $R_c=8$ and (b) $R_a=\beta R_b$ using $R_a=2$, $R_b=4$, and $R_c=0$. The profiles are shown for increasing time from $t=500$ up to $t=3000$ with an interval of 500 between successive profiles and $L_x=512$. The dot-dashed curves correspond to the initial density profiles.

the magnitude of the density gradient ahead of the reaction front becomes larger than the magnitude of the density gradient behind the reaction front.

In the very special case when $R_a=\beta R_b$ and $R_c=(1+\beta)R_b$ then the RD density is equal everywhere and this is the only point in the parameter space for which no convection is present in the RDC system.

It is also useful to examine the large time solutions to this problem. As we have equal diffusion coefficients, the solutions given by Koza (1996) and Sinder and Pelleg (2000) reduce to

$$[\overline{a},\overline{b},\overline{c}]=\begin{cases}\left[1-\dfrac{1+\beta}{2}\operatorname{erfc}(-\eta),0,\dfrac{\beta}{2}\operatorname{erfc}(-\eta)\right] & \text{for } \eta<C_f/2\\ \left[0,\beta-\dfrac{1+\beta}{2}\operatorname{erfc}(\eta),\dfrac{1}{2}\operatorname{erfc}(\eta)\right] & \text{for } \eta>C_f/2\end{cases}$$

where $C_f/2=\operatorname{erfc}^{-1}(2\beta/(1+\beta))$ which is a monotonic decreasing function of β and at the reaction front $\overline{c}$ takes its maximum value of $\beta/(1+\beta)$. Using these large time asymptotic solutions we can construct the RD density profile

$$\overline{\rho}=\begin{cases}R_a+\dfrac{1}{2}(\beta R_c-(1+\beta)R_a)\operatorname{erfc}(-\eta) & \text{for } \eta<C_f/2\\ \beta R_b+\dfrac{1}{2}(R_c-(1+\beta)R_b)\operatorname{erfc}(\eta) & \text{for } \eta>C_f/2\end{cases}$$

which reveals that the RD density profile has a positive gradient to the left of the reaction front if and only if $\beta R_c>(1+\beta)R_a$. Similarly, the RD density profile has a positive gradient to the right of the reaction front if and only if $R_c<(1+\beta)R_b$. Finally, the initial density is largest for $x>0$ if and only if $\beta R_b>R_a$. Thus the (R_c,R_b) parameter space can be divided into six different regions classified by the resulting RD density profile, see Fig. 4. If $\beta=1$, we recover the results in Rongy et al. (2008).

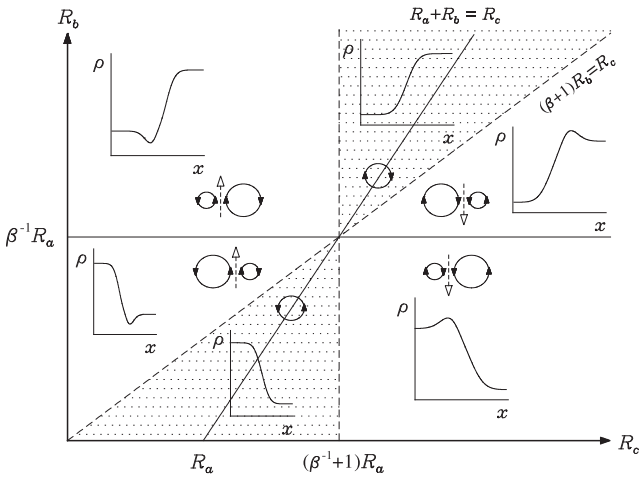

Fig. 4. Classification of the different RDC dynamics in the (R_c,R_b) parameter plane at fixed R_a. Typical density profiles in the absence of convection as well as a sketch of the expected vortex dynamics are illustrated within the corresponding regions. The shaded region corresponds to monotonic density profiles with one single vortex. Outside the shaded region, non-monotonic density profiles and two vortices are obtained. The arrow on the circles indicate the rotation direction of the vortex. The dashed arrow indicates whether C is rising or sinking in the gravity field.

4. Effects of buoyancy-driven convection on A+B→C fronts

Eqs. (8)–(12) have been numerically integrated subjected to the boundary and initial conditions described in Section 2. The model includes five dimensionless parameters: the three Rayleigh numbers $R_{a,b,c}$, of the species involved in the chemical reaction, the layer thickness, L_z, and the initial reactant concentration ratio, $\beta=b_0/a_0$. The layer length L_x is taken long enough not to affect the results, typically $L_x=1024$ here. Without loss of generality we can consider systems with a reactant B initially less concentrated than A ($\beta\le 1$, $b_0\le a_0$) for which the RD front moves to the right ($x_f\ge 0$). Throughout most of this study, the layer thickness and the ratio of initial reactant concentrations are usually fixed to $L_z=10$ and $\beta=0.5$, respectively.

4.1. Fluid dynamics

By examining numerical solutions for various sets of Rayleigh numbers, we found that the number of convective rolls, their relative size and rotational direction can all be predicted on the basis of the depth-averaged density profiles $\langle\rho\rangle$, which present the same symmetry and monotonous properties as the RD density profiles. All depth-averaged quantities are defined as

$$\langle\phi\rangle(x,t)=\frac{1}{L_z}\int_0^{L_z}\phi(x,z,t)dz,$$

where ϕ denotes the field being averaged. Indeed, as stated earlier, the flow field is driven by the horizontal density gradient, so that two convective rolls are present when $\langle\rho\rangle$ is non-monotonic, i.e. its gradient $\langle\rho\rangle_x$ changes sign in the x-direction. On the contrary, only one convective roll is present when $\langle\rho\rangle$ is monotonic, i.e. its gradient does not change sign along x, as shown in Fig. 4.

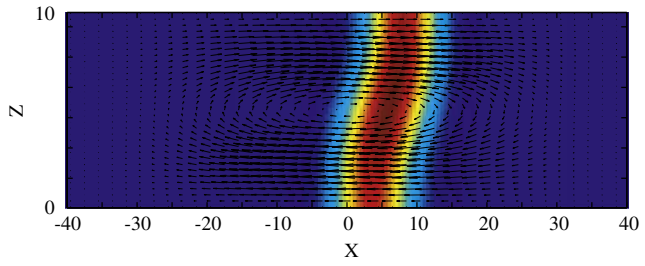

Fig. 5. Focus on the symmetric convection roll centered on $x=0$ shown at $t=50$ for $R_a=2$, $R_b=6$, $R_c=8$, $L_z=10$ and $\beta=0.5$. The fluid velocity field is superimposed on a 2D plot of the production rate which ranges between its maximum value shown in red, $\langle ab\rangle_{max}=6.18\times10^{-3}$, localized at $x=X_f>0$ and $z=L_z/2$ and its minimum value, 0, shown in blue. The z-direction has been magnified and the velocity vectors are here doubled compared to their effective length. (For interpretation of the references to color in this figure legend, the reader is referred to the web version of this article.)

Fig. 4 illustrates that, if R_c lies between $(1+\beta^{-1})R_a$ and $(1+\beta)R_b$, then the RD density profile is monotonic and the RDC system has a single convective roll centered around the reaction front. This roll turns clockwise for $R_b>\beta^{-1}R_a$ and anti-clockwise for $R_b<\beta^{-1}R_a$. If R_c is greater than the maximum of $(1+\beta^{-1})R_a$ and $(1+\beta)R_b$ then the RD profile exhibits a local maximum so that the density is greatest near the reaction front and the RDC system has two convective rolls with the fluid falling downwards at the reaction front. Similarly the RD profile exhibits a local minimum when R_c is less than the minimum of $(1+\beta^{-1})R_a$ and $(1+\beta)R_b$ so that the density is smallest near the reaction front and the RDC system has two convective rolls with the fluid rising upwards at the reaction front.

An example of a symmetric convective roll is presented in Fig. 5 for a case such that $\beta<1$ and $R_a+R_b=R_c$ for which the RD density profile is antisymmetric and monotonic which corresponds to the tilted straight line in Fig. 4. In the presence of convection, the density profiles are still found to be antisymmetric about $x=0$ at every height of the layer and for all times. The corresponding fluid flow therefore consists of a single symmetric convective roll whose center is located at $x=0$ for all time. Finally the initially planar reaction front has been deformed by the convection across the layer. The center of the reaction front is moving to the right in Fig. 5, due to $\beta<1$, so that the position of the maximum production rate is moving away from the center of the convective roll which remains at $x=0$ in this case. We also find that the presence of convection initially accelerates the reaction front with regard to the pure RD situation. Illustrations of asymmetric convection rolls can be found in Rongy et al. (2008).

The presence of convection is found to always increase the total amount of C being produced per unit of time and the stronger the intensity of the fluid flow the more C is produced. When $\beta=1$ and R_a and R_b are fixed, then the amount of product produced is minimized when the quantity $|R_c-R_a-R_b|$ is minimized, due to the symmetric production rate about the line $R_c=R_a+R_b$.

4.2. Reaction front dynamics

The position of the reaction front, defined in 1D systems as the point where the production rate ab is maximum, is here defined for our 2D geometry as X_f, the point where the depth-averaged production rate $\langle ab\rangle$ reaches its maximum. It is important to recall that as the reactants have equal diffusion coefficients the RD front cannot change direction, it is either stationary when $\beta=1$ or continuously moves away from $x=0$ otherwise. Although RD fronts can exhibit exotic behavior, the front direction reversal

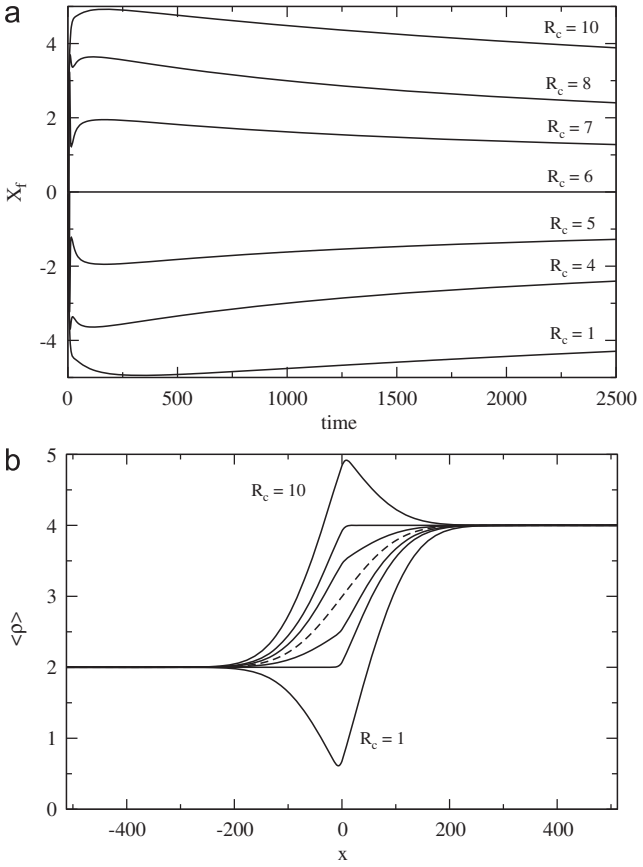

Fig. 6. (a) Position of the RDC front X_f against time with $R_a=2$, $R_b=4$ and various values of R_c. (b) Depth-averaged density profiles along x at $t=3000$ for the same parameters as in (a), i.e. $R_c=1$, 4, 5, 6, 7, 8, 10 from bottom to top. The broken curve represents the antisymmetric density profile obtained for $R_c=6$. Both results used a layer thickness $L_z=10$ and $\beta=1$.

phenomena that will be obtained in this study are not related to the reversal that one can obtain with unequal diffusion coefficients but are instead intrinsically due to convection.

4.2.1. Reaction front dynamics for $\beta=1$

When $\beta=1$, the RD front is stationary, i.e. $x_f=0$, so that any change in the RDC front, X_f, can be attributed solely to convective effects. In this case Rongy et al. (2008) found via a numerical parametric study that convection causes the reaction front to initially move to the region with the smallest density gradients, i.e. away from the side where the fluid flow is most intensive. This behavior is analogous to that of the RD front which moves away from the side where the diffusive flux is largest. Thus convection causes the reaction front to move to the right when either B is heavier than A with C heavier than the sum of A and B (i.e. $R_c>R_a+R_b>2R_a$) or B is lighter than A with C lighter than the sum of A and B (i.e. $R_c<R_a+R_b<2R_a$). Conversely, the reaction front moved to the left when either $R_c<R_a+R_b<2R_b$ or $R_c>R_a+R_b>2R_b$.

Rongy et al. (2008) showed that when $\beta=1$, in the two particular cases, $R_a=R_b$ and $R_c=R_a+R_b$, the density profile is symmetric and antisymmetric, respectively, and the reaction front is therefore immobile even in the presence of convection. An asymmetric fluid flow, on the contrary, always leads to the motion of the front. These findings are illustrated in the case where the reactant A is lighter than the reactant B in Fig. 6(a) where X_f is plotted in time. The understanding of the dynamics of X_f is

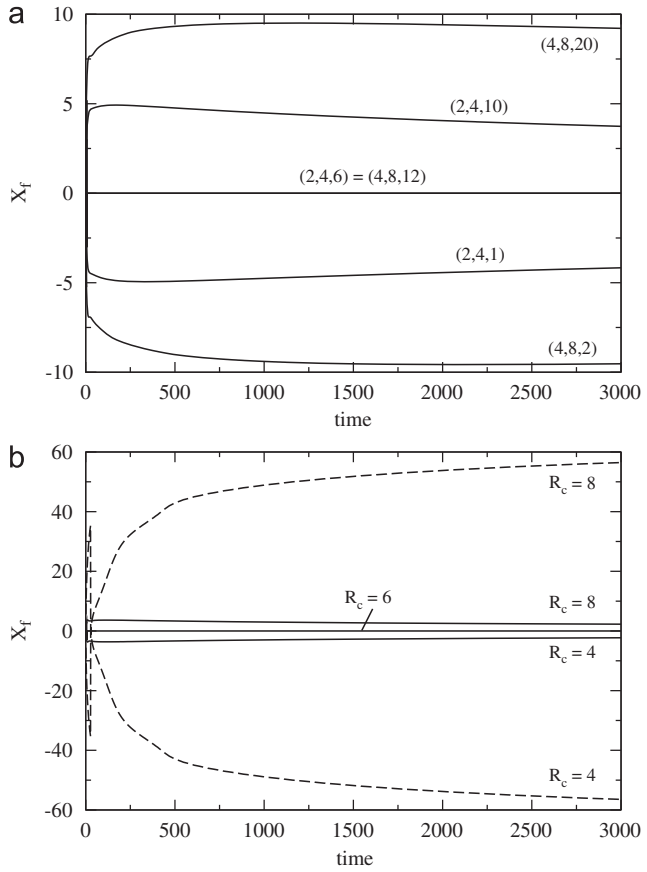

Fig. 7. Position of the RDC front X_f against time for $\beta = 1$ and for (a) $L_z = 10$ and six different values of (R_a, R_b, R_c) and (b) $R_a = 2$, $R_b = 4$ and three different values of R_c each for both $L_z = 10$ (solid curves) and $L_z = 20$ (broken curves). For the particular values $R_c = 6$ corresponding to a non-moving front, the curves for $L_z = 10$ and $L_z = 20$ are superimposed.

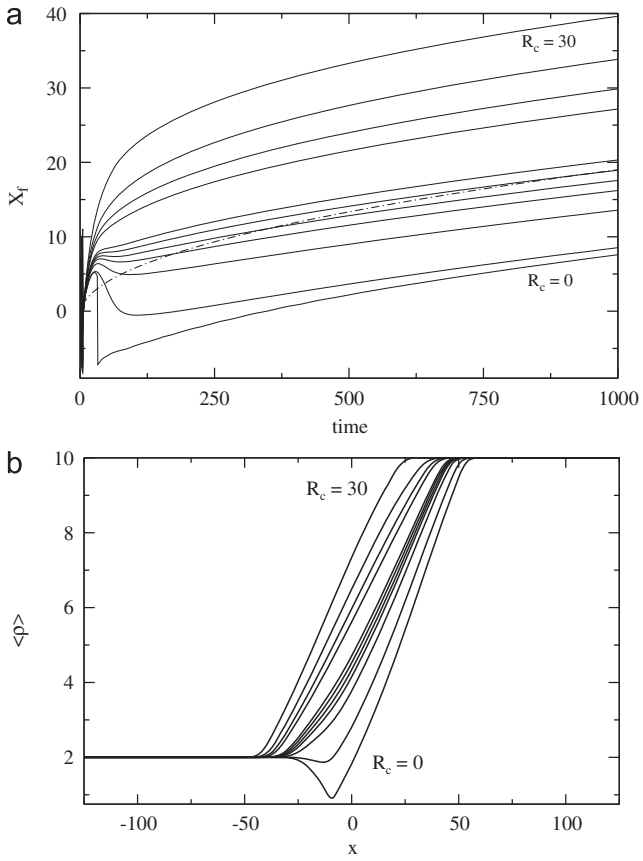

Fig. 8. Position of the reaction front X_f against time (a) and depth-averaged density profiles along x at $t = 30$ (b) for $R_a = 2$, $R_b = 20$ and various R_c: $R_c = 0$, 5, 10, 12, 13, 14, 15, 20, 22, 25, 30 from bottom to top. The layer thickness $L_z = 10$ and $\beta = 0.5$. In (a) the dot-dashed curve corresponds to the RD propagation.

assisted by the corresponding averaged density profiles $\langle \rho \rangle$ at $t = 3000$ in Fig. 6(b). When $R_c = 6$, so that $R_c = R_a + R_b$, the density profile is monotonic and antisymmetric leading to a convection roll with equal intensity on the left and right sides and therefore to a stationary front ($X_f = 0$, $\forall t$). When the density gradient is stronger on the right side ($R_c < 6$), convection is also more intense on this side pushing the reaction front in the opposite direction leading to $X_f < 0$. The reverse is true for $R_c > 6$. The motion of the front and the maximum fluid velocity increase as $|R_c - R_a - R_b|$ is increased. Hence, the evolution of X_f for a given triplet of parameter values (R_a, R_b, R_c) can be obtained by symmetry from the situation at (R_a, R_b, $2R_a + 2R_b - R_c$), as seen in Fig. 6(a).

After a sufficient amount of time, the driving force of the convection decreases as the density gradients begin to weaken in time. Hence, the reaction front slows down and eventually changes direction to return to its initial position $X_f = 0$ as predicted by the RD theory. Moreover, the deformations across the layer decay with the front tending to a planar profile. We have checked that the direction changes indeed arise from the weakening of convection by artificially setting $R_{a,b,c} = 0$, i.e. stopping the flow, after some time. We observe that X_f then returns to zero as expected.

In Fig. 7(a), X_f is plotted in time for various triplets of (R_a, R_b, R_c) with $\beta = 1$ which shows that increasing $R_{a,b,c}$ leads to a reaction front traveling further as well as causing a delay in the time at which the reaction front changes direction. We note that our analytical findings have been verified numerically for different sets of values of $R_{a,b,c}$ (≤ 100) confirming that all the features of the RDC dynamics are determined by the RD profiles and the relative values of the Rayleigh numbers. Multiplying these numbers by the same factor (> 1) gives rise to the same qualitative dynamics but with more intense convection and larger $|X_f|$ (see Fig. 7(a)).

In Fig. 7(b), X_f is plotted in time for fixed R_a, R_b, $\beta = 1$ and for different values of R_c and L_z showing that increasing L_z leads to a reaction front traveling further as well as causing a delay in the time at which the reaction front changes direction. Since the domain height, L_z, affects the intensity of convection but not the structure of the flow driven by the density gradients, all the results and especially the classification of the different possible regimes are independent of the specific value of L_z. Nevertheless, the larger L_z, the stronger the convection and the larger $|X_f|$ (see Fig. 7(b)).

We can therefore conclude that, when $\beta = 1$, increasing $R_{a,b,c}$, while maintaining their ratio, or increasing L_z both lead to enhanced convection, an increase in the displacement of the reaction front, and an increase in the amount of C produced per unit time. The direction of front propagation is however determined only by the relative values of $R_{a,b,c}$.

4.2.2. *Reaction front dynamics for $\beta < 1$*

Next, we investigate the dynamics of X_f in the case of unequal initial concentrations with $\beta < 1$ so that the RD front moves to the

right, i.e. $x_f > 0$. The RDC dynamics are more subtle than for $\beta = 1$ since the fluid flow is now superimposed on an already moving RD front. Thus the RD system does not provide a simple criterion on the direction of the reaction front in the RDC system.

In the presence of asymmetric convection we find that X_f can behave exotically. As $\beta < 1$, in the presence of sufficiently weak convection the reaction front moves to the right, i.e. $X_f > 0$. However, by suitably choosing the parameter values of R_a, R_b and R_c to make the fluid flow more intense on the right hand side than on the left hand side the convective flow is able to reverse the direction of the reaction front as illustrated in Fig. 8(a) where X_f is plotted against time for fixed $R_a < \beta R_b$ with $\beta = 0.5$ and various values of R_c. In Fig. 8(b) the corresponding depth-averaged density profiles at an early time ($t = 30$) are also presented. One observes that for R_c greater than a critical value R_c^{cr} (≈ 14 for the parameter values in Fig. 8(a)) the reaction front continuously propagates to the right. However, for R_c below this critical value, although the reaction front initially moves to the right, around $t = 30$ it starts to move to the left. Further in time the convective forces begin to decay and the reaction front changes direction again propagating to the right.

The results in Fig. 8 can be physically explained as follows. For small times there is very little product present and very little of the reactants have been consumed so that the RD density profile is anti-symmetric, thus the induced convection will enhance the propagation of the RD front without affecting its direction. As time increases, the concentration of the product increases and more of the reactants are consumed, thereby increasing the asymmetry of the density profiles along x and hence increasing the intensity of the resulting asymmetric flow, as long as $R_c \neq R_a + R_b$. As $R_a < \beta R_b$, if R_c is sufficiently small then the density gradient becomes much stronger on the right hand side so that the reaction front starts to propagate towards the left where the fluid flow is less intense. When R_c is increased, the propagation in the reverse direction favored by convection is weakened as the asymmetry of the density profiles is reduced. At $R_c = R_c^{cr}$ no change in direction is observed since the fluid flow is not asymmetric enough to overcome the underlying RD direction of propagation. We notice that the value of $R_c^{cr} < R_a + R_b$ since at $R_c = R_a + R_b$ the density profiles are anti-symmetric along x so that convection cannot affect the direction of propagation of the reaction front.

For all Rayleigh numbers, the front propagates to the right in the large time limit because convection gets weaker in time and diffusion takes over again since the concentration gradients and hence the density gradients decay. This explains the second change in propagation direction[1] when $R_c < R_c^{cr}$. However, the propagation remains affected by the fluid flow with a deformed reaction front across the layer and X_f scales in time like t^α different from the $t^{1/2}$ scaling predicted in the diffusive limit. Table 1 reports that the exponent α of the scaling of X_f in time is larger than the RD value 0.5 when there is an early time front direction reversal while $\alpha < 0.5$ when the fluid flow is not asymmetric enough to overcome the diffusion-driven propagation. α approaches 0.5 when R_c converges to the threshold value R_c^{cr} situated between 13 and 14 for $R_a = 2$ and $R_b = 20$ (see Fig. 8(a) and Table 1). We note that these exponents get closer to 0.5 when time increases due to the dampening of convection.

[1] We note that for all the Rayleigh numbers considered in this study, the direction of front propagation can have an additional switch at early times as can be observed for $\beta = 1$ (cf. Fig. 7(b)). This arises from the fact that in the short time limit the depth-averaged production rate presents two local maxima of similar amplitude. However, one of them rapidly disappears in favor of the other. The double change in propagation direction observed for $R_a = 2$, $R_b = 20$ and $R_c < 14$ is characterized by two values of time t for which $dX_f/dt = 0$ and has nothing to do with the rapid changes occurring at earlier times.

Table 1
Exponent α of the power law fit to numerical data for $X_f \sim t^\alpha$ between $t = 1500$ and 3000 as a function of R_c, for $R_a = 2$ and $R_b = 20$.

R_c	0	5	10	12	13	14	15	20	22	25	30
α	0.85	0.82	0.62	0.55	0.52	0.49	0.47	0.38	0.35	0.32	0.28

The same reasoning also applies to the case $R_a > \beta R_b$ where now R_c must be chosen sufficiently larger than $R_a + R_b$ so that the induced fluid flow is sufficiently asymmetric to eventually overcome the initial RD flux to make the front propagate to the left for intermediate times.

We find that the double switch in propagation direction is always possible as long as $\beta \neq 1$, $R_a \neq \beta R_b$ and R_c is chosen appropriately. For equal diffusion coefficients, the small time asymptotic RD limit yields $x_f = (1-\beta)t^{3/2}/(2\sqrt{\pi})$ see Trevelyan (2009) whilst the large time asymptotic limit yields $x_f = 2\sqrt{t}\,\mathrm{erfc}^{-1}(2\beta/(1+\beta))$. Thus both the small and large time asymptotic limits of x_f have the same sign. As the fluid flow is driven by gravity and the flow is initially stationary, for sufficiently small times the velocities can be neglected and the reaction front will follow the RD theory. Similarly, for sufficiently large times, the fluid flow weakens and so eventually can be neglected so that the reaction front will again follow the RD theory. Hence, if the fluid flow is sufficiently strong to change the direction of the reaction front once, then ultimately the reaction front must change direction a second time, when $\beta \neq 1$.

4.2.3. *Effect of parameters on front propagation reversal*

Let us now consider the influence of the different parameters of the problem on the occurrence of a front direction reversal. As seen in Fig. 8, the increase of R_c leads to a decrease of the reverse propagation tendency. Beyond a certain threshold R_c^{cr}, no reverse propagation occurs. When R_b is increased at fixed $R_a < \beta R_b$ and R_c, the propagation of the front in the reverse direction is more important, arising from a larger asymmetry of the density profiles along x. The threshold value of R_c is therefore larger. As an example a double reversal of the front direction is found to occur when $R_a = 2$, $R_b = 30$ and $R_c < R_c^{cr} \approx 20$ for $\beta = 0.5$. Similarly, an increase of R_a keeping $R_a < \beta R_b$ and R_c constant reduces the propagation in reverse direction by reducing the asymmetry of the density profiles along x.

Fig. 9 illustrates the influence of the layer thickness L_z and of the initial ratio of reactant concentrations β on the propagation direction. When L_z decreases, the intensity of convection decreases and so does the propagation in the reverse direction. For the Rayleigh numbers in Fig. 9, no reversal is observed when $L_z = 5$. This situation is different from the case $\beta = 1$ where the layer thickness only affects the dynamics of the system quantitatively but not qualitatively. Here, as the RD front is already propagating, convection needs to overcome the diffusion-driven propagation to induce a front direction change. Therefore, the qualitative behavior of the system depends not only on the characteristics of the flow but also on its intensity. When β increases up to one, the difference in reactant concentrations decreases. The driving force of the RD system is therefore less pronounced leading to a less important propagation. As a result, for the same asymmetric fluid flow, the front reversal is weaker when β decreases, i.e. when convection has to overcome a stronger diffusive flux (see Fig. 9(b)).

To summarize our parametric study, we find that the distance traveled by the front in the reverse direction and the threshold value $R_c^{cr} = R_c^{cr}(R_a, R_b, L_z, \beta)$, below which this reversal is observed,

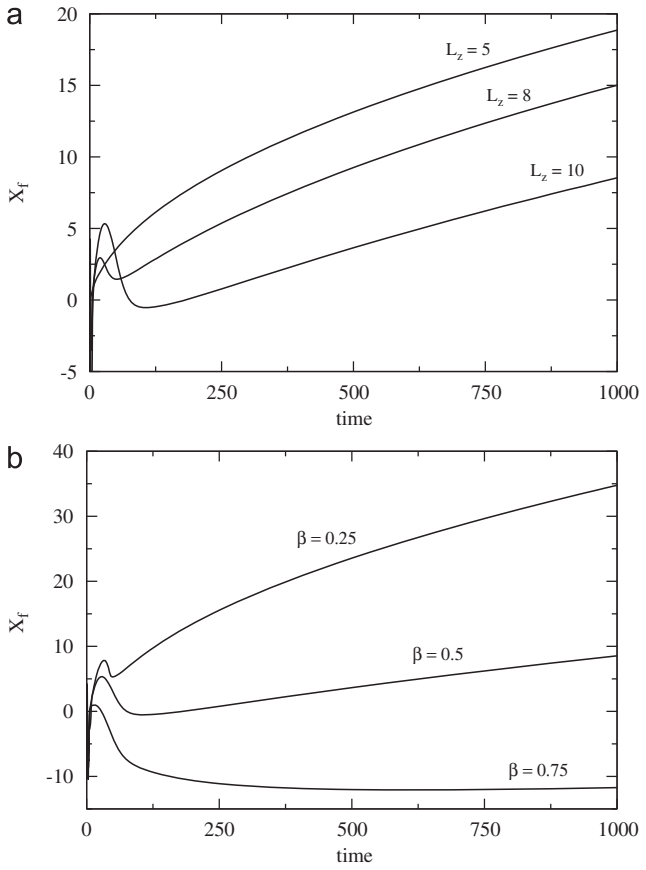

Fig. 9. Position of the reaction front X_f against time for $R_a = 2$, $R_b = 20$ and $R_c = 5$. (a) $\beta = 0.5$ and the reversal increases with L_z. (b) $L_z = 10$ and the reversal increases with β.

are increasing functions of R_b, L_z and β, and decreasing ones of R_a for $R_a < \beta R_b$.

In conclusion, the direction of propagation of the reaction front is governed after a long time by the diffusive limit, however, for short to intermediate times the presence of convection can drastically alter the front propagation and even reverse its direction. The front is deformed across the layer and the scalings obtained by the RD analysis are no longer valid.

4.3. Experimental values of physical parameters

Throughout this paper, we have used dimensionless variables to describe the system's dynamics. The various chemical reactions that have been used to verify the RD scalings predicted by Gálfi and Rácz (1988) could be used to compare with our theoretical results. These reactions have kinetic constants ranging between $k \sim 10^{-1}$ and $\sim 10^6\,\mathrm{M^{-1}\,s^{-1}}$, see Baroud et al. (2003), Koo and Kopelman (1991) and Taitelbaum et al. (1992), which, along with the initial reactant concentration a_0 between 5.0×10^{-5} M and 1.0×10^{-3} M, gives characteristic times $\tau_c = 1/(ka_o)$ varying between $\tau_c = 10^{-3}$ s and $\tau_c = 2 \times 10^5$. The diffusion coefficients of the involved species are equal to $D \sim 3.0 - 8.0 \times 10^{-6}\,\mathrm{cm^2/s}$, see Baroud et al. (2003), Koo and Kopelman (1991) and Taitelbaum et al. (1992), corresponding to characteristic length scales $L_c = \sqrt{D\tau_c}$ running between 5.5×10^{-4} mm and 1.2 cm. The large range of possible dimensional scales is the reason why we have conducted the present analysis in dimensionless variables.

5. Conclusions

The dynamics of A+B→C fronts in horizontal solution layers can be influenced by buoyancy-driven convection if A, B and C contribute differently to the density of the aqueous solution. By numerically integrating the 2D incompressible Stokes equations coupled to reaction–diffusion–convection equations for the three chemical species concentrations, we show that the presence of convection deforms the reaction front across the layer and radically affects its propagation properties. Such convective motions can lead to front propagation even in the case of equal diffusion coefficients and equal initial concentrations of reactants for which reaction–diffusion models predict a stationary front. We show numerically and analytically that the dynamics in the presence of convection can in that case be actually predicted from the properties of the simple one-dimensional RD density profile across the front. We have shown that if the density is symmetric ($R_a = R_b$) or antisymmetric ($R_c = R_a + R_b$), the induced fluid flow is symmetric about the reaction front which remains immobile even in the presence of convection. On the contrary, if the density is asymmetric, the front moves in the direction of the smallest density gradient, i.e. the weakest flow. In the case of reactants with different initial concentrations, the presence of a chemically induced fluid flow can lead to an acceleration and even to a reversal of the front propagation direction in time. In all cases, convection eventually fades away in time because the concentration gradients decrease and the direction of front propagation is therefore eventually controlled by the difference in initial reactant concentrations as in the RD system.

Several extensions of this work could be envisaged. First, the case of different diffusion coefficients of the reactants (and ultimately of the product) could be considered to obtain a complete picture of all the various possible dynamics, starting with the particular case, $a_0\sqrt{D_a} = b_0\sqrt{D_b}$, for which the RD front is non-moving. It will probably not be possible to predict all the dynamics analytically since criteria on the Rayleigh numbers for the RD density profile to be symmetric/monotonic are hard to find without resorting to numerics. Moreover, the properties of the density profiles might depend on time and on the presence of convection oppositely to the case of $D_a = D_b$. A two-phase system modeling the reaction between A and B initially separated in immiscible solutions would allow a comparison of the theoretical results with the experiments carried out by Shi and Eckert (2006) and to model non-agitated extraction phenomena in the presence of a chemical reaction. Eventually, if the layer is open to air or in the latter case of immiscible liquids, chemically induced Marangoni convection could be coupled to the buoyancy effects.

Acknowledgments

L.R. is supported by a BAEF fellowship and PMJT by a Prodex contract. A.D. acknowledges financial support from Prodex (Belgium), FNRS and from the "Communauté française de Belgique" ("Actions de Recherches Concertées" program).

References

Baroud, C.N., Okkels, F., Ménétrier, L., Tabeling, P., 2003. Reaction–diffusion dynamics: confrontation between theory and experiment in a microfluidic reactor. Phys. Rev. E 67, 060104.

Cornell, S.J., Koza, Z., Droz, M., 1995. Dynamic multiscaling of the reaction–diffusion front for mA+nB→0. Phys. Rev. E 52, 3500.

Cornell, S.J., 1995. Refined simulations of the reaction front for diffusion-limited two-species annihilation in one dimension. Phys. Rev. E 51, 4055–4064.

Danckwerts, P.V., 1950. Unsteady-state diffusion or heat-conduction with moving boundary. Trans. Faraday Soc. 46, 701–712.
Epstein, I.R., Pojman, J.A., 1998. An Introduction to Nonlinear Chemical Dynamics. Oxford University Press, Oxford.
Gálfi, L., Rácz, Z., 1988. Properties of the reaction front in an A+B→C type reaction–diffusion process. Phys. Rev. A 38, 3151.
Jiang, Z., Ebner, C., 1990. Simulation study of reaction fronts. Phys. Rev. A 42, 7483.
Koo, Y.-E.L., Li, L., Kopelman, R., 1990. Reaction front dynamics in diffusion-controlled particle–antiparticle annihilation: experiments and simulations. Mol. Cryst. Liq. Cryst. 183, 187.
Koo, Y.-E.L., Kopelman, R., 1991. Space- and time-resolved diffusion-limited binary reaction kinetics in capillaries: experimental observation of segregation anomalous exponents and depletion zone. J. Stat. Phys. 65, 893.
Koza, Z., 1996. The long-time behavior of initially separated A+B→0 reaction–diffusion systems with arbitrary diffusion constants. J. Stat. Phys. 85, 179.
Koza, Z., Taitelbaum, H., 1996. Motion of the reaction front in the A+B→C reaction–diffusion system. Phys. Rev. E 54, R1040–R1043.
Larralde, H., Araujo, M., Havlin, S., Stanley, H.E., 1992. Reaction front for A+B→C diffusion–reaction systems with initially separated reactants. Phys. Rev. A 46, 855–859.
Park, S.H., Parus, S., Kopelman, R., Taitelbaum, H., 2001. Gel-free experiments of reaction–diffusion front kinetics. Phys. Rev. E 64, 055102(R).
Rongy, L., De Wit, A., 2006. Steady Marangoni flow traveling with chemical fronts. J. Chem. Phys. 124, 164705.
Rongy, L., Goyal, N., Meiburg, E., De Wit, A., 2007. Buoyancy-driven convection around chemical fronts traveling in covered horizontal solution layers. J. Chem. Phys. 127, 114710.
Rongy, L., Trevelyan, P.M.J., De Wit, A., 2008. Dynamics of A+B→C reaction fronts in the presence of buoyancy-driven convection. Phys. Rev. Lett 101, 084503.
Shi, Y., Eckert, K., 2006. Acceleration of reaction fronts by hydrodynamic instabilities in immiscible systems. Chem. Eng. Sci. 61, 5523.
Sinder, M., Pelleg, J., 2000. Asymptotic properties of a reversible A+B↔C static reaction–diffusion process with initially separated reactants. Phys. Rev. E 62, 3340.
Taitelbaum, H., Havlin, S., Kiefer, J.E., Trus, B., Weiss, G.H., 1991. Some properties of the A + B→ reaction-diffusion system with initially separated components. J. Stat. Phys. 65, 873.
Taitelbaum, H., Koo, Y.-E.L., Havlin, S., Kopelman, R., Weiss, G.H., 1992. Exotic behavior of the reaction front in the A+B→C reaction–diffusion system. Phys. Rev. A 46, 2151.
Taitelbaum, H., Koza, Z., 2000. Reaction-diffusion processes: exotic phenomena in simple systems. Phys. Rev. A 285, 166.
Trevelyan, P.M.J., Strier, D.E., De Wit, A., 2008. Analytical asymptotic solutions of nA+mB→C reaction–diffusion equations in two-layer systems: a general study. Phys. Rev. E 78, 026122.
Trevelyan, P.M.J., 2009. Analytical small time asymptotic properties of A+B→C. Phys. Rev. E. in press.
Vasquez, D.A., Littley, J.M., Wilder, J.W., Edwards, B.F., 1994. Convection in chemical waves. Phys. Rev. E 50, 280.
Vladimirova, N., Rosner, R., 2003. Model flames in the Boussinesq limit: the effects of feedback. Phys. Rev. E 67, 066305.
Yen, A., Koo, Y.-E.L., Kopelman, R, 1996. Experimental study of a crossover from nonclassical to classical chemical kinetics: an elementary and reversible A+B↔C reaction–diffusion process in a capillary. Phys. Rev. E 54, 2447–2450.